Enhanced thermoelectric properties of flexible aerosol-jet printed carbon nanotube-based nanocomposites

Canlin Ou, Abhijeet L. Sangle, Thomas Chalklen, Qingshen Jing, Vijay Narayan, and Sohini Kar-Narayan

Citation: APL Materials **6**, 096101 (2018); doi: 10.1063/1.5043547
View online: https://doi.org/10.1063/1.5043547
View Table of Contents: http://aip.scitation.org/toc/apm/6/9
Published by the American Institute of Physics

APL MATERIALS **6**, 096101 (2018)

Enhanced thermoelectric properties of flexible aerosol-jet printed carbon nanotube-based nanocomposites

Canlin Ou,[1] Abhijeet L. Sangle,[1] Thomas Chalklen,[1] Qingshen Jing,[1] Vijay Narayan,[2] and Sohini Kar-Narayan[1,a]
[1]*Department of Materials Science and Metallurgy, University of Cambridge, 27 Charles Babbage Road, Cambridge CB3 0FS, United Kingdom*
[2]*Department of Physics, Cavendish Laboratories, University of Cambridge, J. J. Thompson Avenue, Cambridge CB3 0HE, United Kingdom*

(Received 10 June 2018; accepted 6 August 2018; published online 5 September 2018)

Aerosol-jet printing allows functional materials to be printed from inks with a wide range of viscosities and constituent particle sizes onto various substrates, including the printing of organic thermoelectric materials on flexible substrates for low-grade thermal energy harvesting. However, these materials typically suffer from relatively poor thermoelectric performance, compared to traditional inorganic counterparts, due to their low Seebeck coefficient, S, and electrical conductivity, σ. Here, we demonstrate a modified aerosol-jet printing technique that can simultaneously incorporate well-dispersed high-S Sb_2Te_3 nanoflakes and high-σ multi-walled carbon nanotubes (MWCNTs) providing good inter-particle connectivity to significantly enhance the thermoelectric performance of poly(3,4-ethylenedioxythiophene) polystyrene sulfonate structures on flexible polyimide substrates. A nominal loading fraction of 85 wt. % yielded a power factor of ~41 μW/mK^2, which is among the highest for printed organic-based structures. Rigorous flexing and fatigue tests were performed to confirm the robustness and stability of these aerosol-jet printed MWCNT-based thermoelectric nanocomposites. https://doi.org/10.1063/1.5043547

Waste heat is generated from many different processes, such as heat from chemical reactions in various industrial activities, moving parts in machineries, combustion of fossil fuels in automobiles, and metallurgical processes, to name a few.[1,2] Even an average adult human body dissipates ~100 W of heat to the surroundings.[3] Therefore, there is tremendous interest in developing efficient thermoelectric materials, which can convert heat into electricity via the Seebeck effect, to harvest waste heat. However, suitable thermoelectric materials that are cost-effective and that can efficiently convert low-grade heat into electricity are rare, and there exist associated difficulties with processing these into easily adaptable, conformable, and/or flexible thermoelectric energy harvesters.[1,3–9] For example, inorganic materials such as tellurides of bismuth and antimony have been found to be suitable particularly for room-temperature applications, but the scarcity and difficulty of processing these materials make them very expensive and, in certain cases, even unsuitable.[4,5,10] Since the 1990s, research in thermoelectrics has thrived through the discovery of new and efficient materials compositions and also through the boost in thermoelectric performance achieved through nanostructuring of materials.[4,5,10–12] At the same time, the explosive growth witnessed by the Internet of Things, including the wearable industry, has brought about new challenges in providing self-powered solutions that can be easily integrated and that are conformable, light, and flexible. For example, wearable thermoelectric generators can be used as energy sources for low-power sensor applications if they are implanted in clothing or worn as patches which cover typically hotter regions of the body such as the forehead and chest.[3,13] For thermoelectric generators which are to be "worn," an important

[a]Email: sk568@cam.ac.uk

technological challenge is making them light-weight and flexible for ergonomic convenience. Therefore, organic materials such as conducting polymers and carbon nanotubes have been studied in great detail in recent years.[14–18] In addition, there have been great advances in polymer processing techniques, which make the large-scale production of these materials possible. However, compared to their inorganic counterparts, organic materials possess relatively poor thermoelectric energy conversion efficiency.[16–18] In this regard, organic-inorganic composites have been shown to overcome some of the difficulties associated with single-phase thermoelectric materials,[11,18,19] and the ability to print these onto flexible substrates is a particularly attractive feature.[9] Insertion of inorganic nanoparticles into an organic matrix has been shown to have the effect of increasing the Seebeck coefficient, S, and the overall power factor (PF = $S^2\sigma$, where S is the Seebeck coefficient and σ is the electrical conductivity). However, introducing inorganic nanoparticles into a conducting organic matrix can also lower the overall conductivity due to poor connectivity between the particles,[9] which is a problem that needs to be overcome in order to achieve even better thermoelectric performance.

In the literature, carbon-based materials, such as graphite and carbon nanotubes (CNTs), have been reported to possess excellent σ and superior tensile strength when integrated into a composite structure. For example, CNTs can be incorporated with conjugated polymers, e.g., poly(3-hexylthiophene) (P3HT)[20] or poly(3,4-ethylenedioxythiophene) polystyrene sulfonate (PEDOT:PSS)[14,21,22] to enhance the overall electrical conductivity. Additionally, the formation of numerous tube–tube connections and CNT-polymer interfaces can significantly scatter phonons and result in lower thermal conductivity κ[14,23] and thus higher thermoelectric figure-of-merit ZT defined as $S^2\sigma T/\kappa$, at temperature T. However, directly printing these materials can be very tricky because of the challenges involved in the ink preparation, such as functionalising the dispersed particles or nanotubes to form a stable suspension, achieving uniform particle size distribution, and tuning their viscosity for smooth printing using the desired printing technique.[1,24,25] We show here that aerosol-jet printing can serve to mitigate most of these critical problems. As compared to contemporary printing techniques such as screen printing,[26–28] ink-jet printing,[29,30] spin-coating,[17,31] and dispenser printing,[32] aerosol-jet printing offers distinct advantages in terms of the possibility of using inks with a very wide range of viscosities.[33] The acceptable particle size can be much larger and less uniform in comparison with other printing techniques such as inkjet printing, which requires very fine feature sizes. Since aerosol-jet printing is an additive manufacturing technique, micropatterning or elaborate lithography techniques are not needed, leading to more efficient usage of materials and flexibility in the device design. Moreover, we show that it is feasible to print composite materials by *in situ* mixing of two different inks through two different atomisers in the aerosol-jet printer setup, namely, ultrasonic and pneumatic atomisers, by which the composition can be easily varied and controlled, as previously reported.[9,33] In the current work, commercially procured multi-walled carbon nanotubes (MWCNTs) were introduced for the first time into aerosol-jet printed thermoelectric nanocomposites by dispersing these in water along with in-house solvothermally synthesised Sb_2Te_3 nanoflakes,[9] followed by atomisation (i.e., formation of an aerosol of the mixture) via the pneumatic atomiser through capillary action-assisted spraying. Separately a PEDOT:PSS ink was atomised via the ultrasonic atomiser by ultrasonic agitation, and the two different atomised aerosols were mixed *in situ* within a customised Y-shaped junction in the desired proportions.[9,33] The mixed aerosol droplets were further carried by N_2 gas to the deposition head and then deposited onto the polyimide substrate for nanocomposite printing, as described in detail in supplementary material S1 and S2.

As reported in previous studies, sodium dodecyl sulphate (SDS) and polyvinylpyrrolidone (PVP) have been mostly used as surfactants and/or binders to disperse and stabilise CNT bundles homogenously within water and also to prevent them from agglomeration, which facilitates the formation of 3D connected networks with enhanced electrical conductivity.[34–36] In our work, these two surfactants were tested during the printing of MWCNTs. However, it was found that adding SDS surfactant (0.1 wt. %) caused the generation of bubbles within the atomiser chamber during the atomisation process, which had a detrimental influence on the ink atomisation and the subsequent printing process. Adding the PVP surfactant, on the other hand, was found to have little effect on the atomisation and printing processes. In addition, the ink atomisation process in the aerosol-jet printing setup itself entailed vigorous stirring and sonication which helped to improve the homogeneous

dispersion of MWCNTs. Therefore, only a very small amount of PVP surfactant (0.5 wt. %) was added here. Figure 1(a) shows the scanning electron microscope (SEM) image of representative printed MWCNTs-PEDOT:PSS nanocomposite lines by aerosol-jet printing, where the printing quality was found to be excellent with well-defined and smooth edges and surfaces, very minimal overspray, and an average line width of ~200 μm. A crack was formed by fracturing the printed nanocomposite to reveal more details inside the nanocomposite, as can be clearly seen in Fig. 1(b). Through the fracture surface, it can been seen that densely populated MWCNTs were embedded within the PEDOT:PSS matrix, which had been partially pulled out due to the cleaving process. Supplementary material Fig. S2(a) illustrates the dispersion mechanism and the printing process of MWCNTs. In addition, Figs. S2(b)–S2(e) reveal different loading wt. % of MWCNTs dispersed homogeneously within the PEDOT:PSS matrix via our customised aerosol-jet printing technique. The high-resolution SEM images in Fig. S3 show that the diameter of these printed MWCNTs was ~230 nm (±65 nm) with the length of ~6.5 μm (±2.3 μm), which matched well with the supplier's specifications and also confirmed that they remained intact after the atomisation and printing processes due to their excellent ductility and stretchability. Following this, Sb_2Te_3 nanoflakes were incorporated into the nanocomposite as well. Figures 1(c)–1(f) compare the morphology of different printed Sb_2Te_3-MWCNTs-PEDOT:PSS nanocomposites loaded with different wt. % of Sb_2Te_3 nanoflakes and MWCNTs in a 50:50 ratio, where a visibly larger amount of Sb_2Te_3 nanoflakes and MWCNTs were seen with increasing loading ratio, as expected. These nanoscale inclusions were uniformly distributed and embedded within the PEDOT:PSS matrix without any segregation of the different phases, thus resulting in the uniform composition of the printed nanocomposite. The analysis of energy dispersive X-ray (EDX) mapping data, shown in Fig. S4, illustrates the spatial distribution of Sb_2Te_3 and MWCNTs within the PEDOT:PSS matrix, where the "S" element indicates the distribution of the PEDOT:PSS matrix and

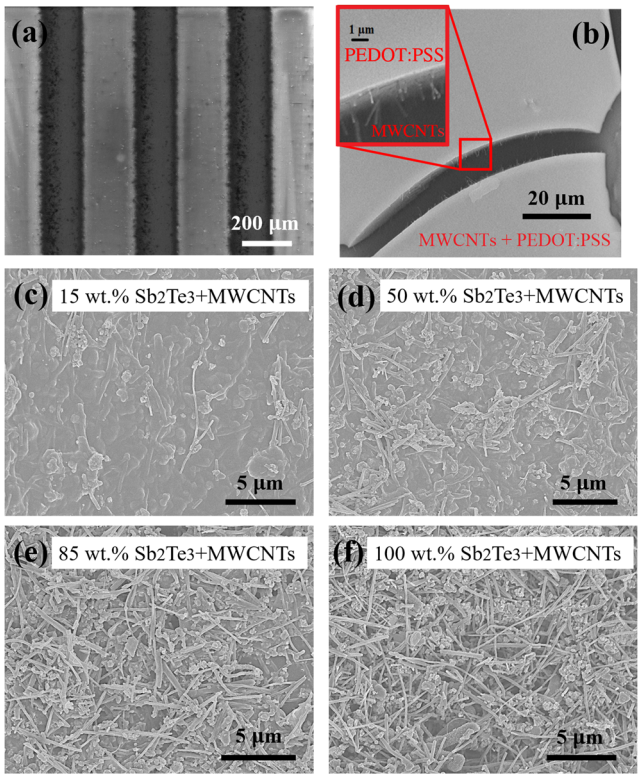

FIG. 1. (a) SEM image of representative printed MWCNTs-PEDOT:PSS nanocomposite lines by aerosol-jet printing. (b) A fracture surface reveals that the MWCNTs were embedded within the PEDOT:PSS matrix and partially pulled out after bending and fracturing the nanocomposite. High-resolution SEM images of printed nanocomposites with different loading ratios of Sb_2Te_3 and MWCNTs within the PEDOT:PSS matrix from (c) 15 wt. %, (d) 50 wt. %, (e) 85 wt. % up to (f) 100 wt. %.

the "Sb" element indicates the distribution of Sb_2Te_3 nanoflakes. This result further confirms the uniformity of the dispersion of Sb_2Te_3 and MWCNTs within the polymer matrix.

Several groups have attempted treating the deposited pristine PEDOT:PSS films by using different chemicals to improve their σ and S.[16,31,37–40] The commonly accepted mechanism is to de-dope the insulating PSS molecules from the conducting PEDOT chains by using different polar solvents.[31] Importantly, CNTs can further improve the σ of the printed PEDOT:PSS-based nanocomposites by forming continuous links between PEDOT islands owing to their superior conductivity and by favorable π-π interactions.[14,21,22] Therefore, printed PEDOT:PSS-based nanocomposite samples with different nanocomposite loading fractions were prepared, followed by surface treatments with polar solvents including ethylene glycol (EG),[16,31,37] dimethyl sulfoxide (DMSO),[31,38] and glycerol (GYL),[41] to investigate their effects on the final thermoelectric properties. Finally, these printed nanocomposites were prepared for thermoelectric property measurement, as described in detail in supplementary material S4.

As can be seen in Figs. 2 and S6, the surface treatment led to a significant improvement in σ, especially seen in the DMSO-treated samples which were found to show an increase in σ by a factor of 5 as compared to the untreated sample. This, therefore, led to the highest power factor

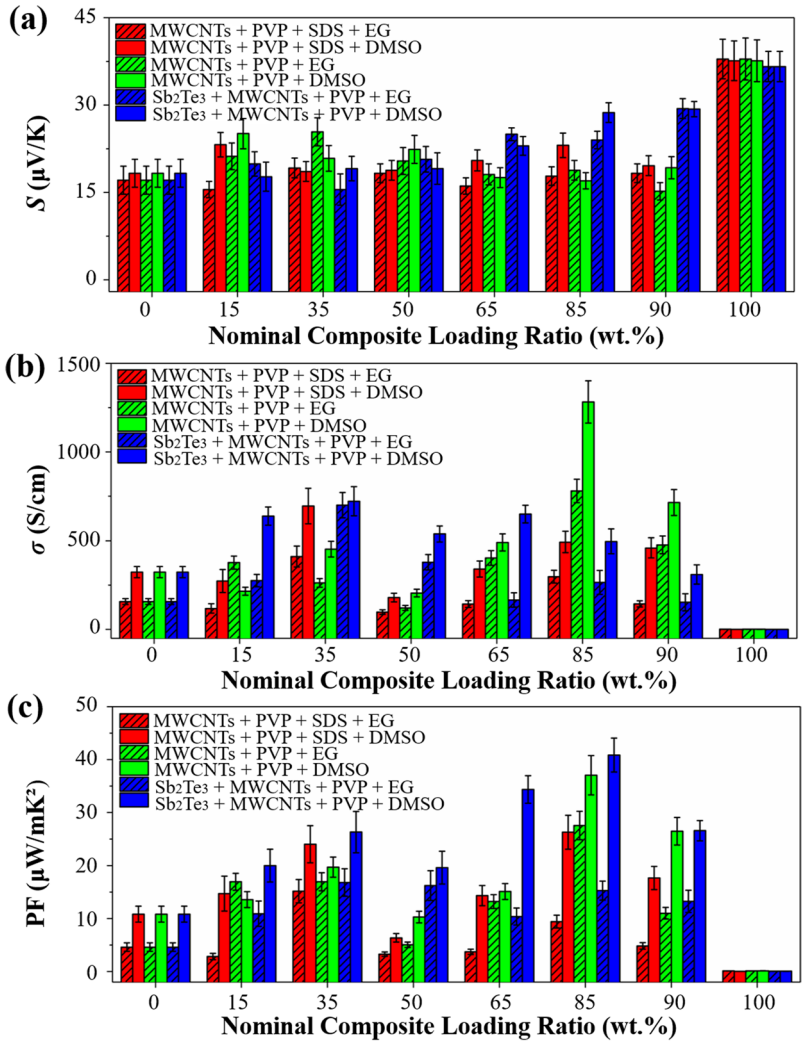

FIG. 2. (a) Seebeck coefficient, (b) electrical conductivity, and (c) power factor of printed PEDOT:PSS-based nanocomposites loaded with different components and compositions and surface-treated with different polar solvents. Error bars indicate the standard deviation of the measured values of two separate printed samples with the same loading components.

(PF) obtained in the samples treated with DMSO. Moreover, it was found that the GYL-treatment was prone to delaminating the printed films off the substrate, and thus this treatment was abandoned in the subsequent investigation. Although the obtained PF was still less than some of the very best results reported,[31] it should be noted that these results were obtained from a different PEDOT:PSS starting material, which has been shown to have vastly superior σ compared to PEDOT:PSS from other vendors as compared in detail in Table S2.[16,18,31,42] We note here that the work from Kim *et al.*[31] has yet to be repeated by any other group. The measured PF in our work nevertheless compared favorably with other reported values based on PEDOT:PSS from similar suppliers.[9,42,43]

When considering the performance of CNT-based composites, the introduction of surfactants is usually best avoided.[44] Figures 2 and S6 indicate that the removal of SDS surfactant can largely improve the final σ and PF values of printed MWCNTs-PEDOT:PSS nanocomposites. Moreover, the added EG/DMSO within the PEDOT:PSS ink could also serve to function as a surfactant to facilitate more homogeneous phase separation between PEDOT:PSS and the loaded inorganic components in the hybrid organic/inorganic composites, as reported by Shin *et al.*[43] Therefore, to further investigate the influence of the PVP surfactant on their final thermoelectric properties, the printed pristine MWCNT samples were heated up to 350 °C to burn away the remaining PVP surfactant. It was found that σ only increased marginally with little change in S. Since the amount of the added PVP surfactant was very small, it had very little influence on the electrical network and quality of contacts within the nanocomposite. In addition, Fig. 2 shows that printed MWCNT films (at 100 wt. %) exhibited very low σ (~1 S/cm) and consequently very poor PF (~0.1 μW/mK^2), which may due to the MWCNT film exhibiting a very porous network as seen in Fig. S3. Therefore, the PEDOT:PSS matrix was essential here, which served as the electrical contact medium between different components of the nanocomposite. Moreover, the addition of Sb_2Te_3 nanoflakes largely enhanced S, albeit with a concomitant decrease in σ, specifically in the high loading ratio region, which resulted in their overall thermoelectric performance (S ~ 29 μV/K, σ ~ 496 S/cm, PF ~ 41 μW/mK^2) slightly exceeding their non-Sb_2Te_3-added counterparts (S ~ 17 μV/K, σ ~ 1282 S/cm, PF ~ 37 μW/mK^2). Although the incorporation of Sb_2Te_3 nanoflakes and MWCNTs within the PEDOT:PSS matrix was seen to be quite dense in Figs. 1(c)–1(e), there were still some poor electrical networks, which arose due to the introduction of relatively lower σ-Sb_2Te_3 nanoflakes creating larger interfacial resistance, whereby the Sb_2Te_3 nanoflakes might block the electrical contact with neighbouring MWCNTs and PEDOT clusters. Nevertheless, these added Sb_2Te_3 nanoflakes could hinder the thermal transport and significantly lower the overall thermal conductivity of printed nanocomposites via the introduction of the phonon-boundary scattering and the large thermal boundary resistance at the interfaces as well-reported in the literature.[10,11,15,45,46] We would therefore expect that nanocomposites with both CNTs and Sb_2Te_3 inclusions will have higher ZT than composites containing only one of these components, particularly in instances where their respective power factors are comparable. Based on the above results, our studies indicate that highly conducting single-walled carbon nanotubes (SWCNTs) or double-carbon nanotubes (DWCNTs) could be used to replace MWCNTs, which would generate up to a couple of orders of magnitude higher σ compared to the currently used MWCNTs.[47,48]

While there has been a considerable number of reports on the improvement of PF or ZT values of current thermoelectrics, the flexibility and robustness of these materials when incorporated into practical applications remain relatively under-reported in the literature. Therefore, rigorous flexing and fatigue tests were devised and conducted on our printed flexible thermoelectric nanocomposites to further quantify their mechanical stability and flexibility under different bending curvatures, as well as their robustness and durability under prolonged flexing cycles. The properties of the printed nanocomposites with the highest PF values were selectively compared here in response to flexing, as shown in Figs. 3(a) and 3(b). Simple manual bending tests [see Figs. S7(a)–S7(c)] and rigorous flexing tests [see Figs. 3(a) and 3(b)] were conducted to estimate their thermoelectric properties under various degrees of curvature, by mounting them onto difference surfaces with difference curvatures, e.g., beaker, test tube, and pen, as illustrated in the inset of Fig. 3(b). It is observed that our printed nanocomposites exhibited an excellent conformability and retained their original smooth surface without forming any visible cracks or deformations after 5 flexing cycles. The electrical resistance of these nanocomposites increased marginally and then plateaued as the curvature increased, suggesting

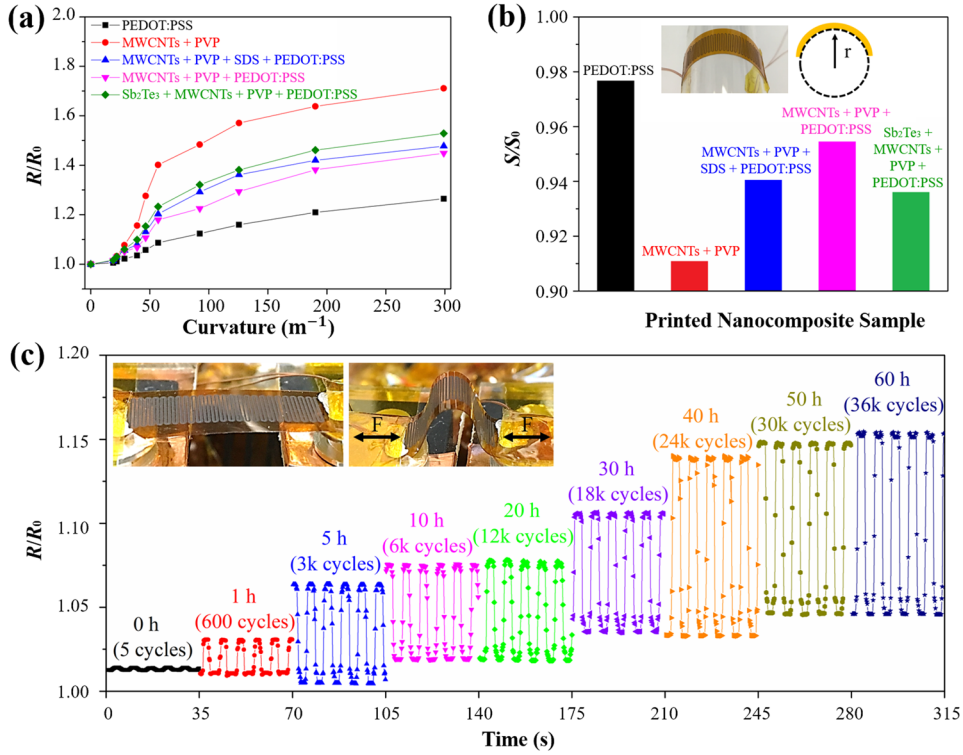

FIG. 3. Flexing test on the printed PEDOT:PSS-based nanocomposites with different loading ratios of MWCNTs and Sb_2Te_3 nanoflakes, where (a) the ratio of the flat-to-flexed resistance was plotted as a function of curvature and (b) the ratio of the flat-to-flexed Seebeck coefficient as a function of loading composition, respectively. Inset: the sample was subjected to a curvature of 190 m^{-1}. (c) Fatigue test of the printed 85 wt. % Sb_2Te_3-MWCNTs-PVP-PEDOT:PSS nanocomposite, continually flexing for 60 h (36k cycles in total) under the application of a periodic compressive stress at a frequency of 0.15 Hz with amplitude of ~10 mm, as shown in the inset, and the data after different flexing cycles were recorded accordingly.

that their excellent flexibility could be attributed to our novel nanocomposite design structure, comprising ductile and conducting MWCNTs networks within the flexible PEDOT:PSS polymer, which serves as a protective matrix to provide greater mechanical support.

A more extensive and continuous fatigue test was subsequently conducted on the printed 85 wt. % Sb_2Te_3-MWCNTs-PVP-PEDOT:PSS nanocomposite by subjecting it to up to 36k continuous flexing cycles, i.e., 60 h of continuous testing at 0.15 Hz, as shown in Figs. 3(c) and S7. The resistance of these flexed nanocomposites did not revert to their original values after released, and it may be due to the formation of very small cracks within the nanocomposite, as can be seen from SEM images taken before and after fatigue testing, shown in Fig. 4. It can be seen that after prolonged flexing and fatigue tests, the nanocomposite film was partially peeled off from the substrate, and there were only a few microcracks formed, which tended to be near the edges of the nanocomposite. Interestingly, the S values of the nanocomposites were found to decrease only slightly after being flexed at very high curvatures ~300 m^{-1}, as can be seen in Fig. 3(b). Furthermore, the S value decreased by only ~15% after the 60 h prolonged fatigue test, which indicates that the observed microcracks did not substantially affect S. These observations confirm the superior flexibility and mechanical stability of the printed flexible nanocomposites as compared with their bulk counterparts. The fatigue result also suggests that after an initial increase in the resistance value (R/R_o), the electrical conductivity remains stable for up to 60 h of testing, which indicates that our printed nanocomposite could be used as a flexible thermoelectric generator to convert the temperature gradients into electricity over a prolonged time. Moreover, it should be noted that our printed nanocomposite was tested over a period of 2 months with negligible degradation in performance. These fatigue results are of significant importance given that such extensive fatigue data are rarely presented in the literature for flexible thermoelectric generators.

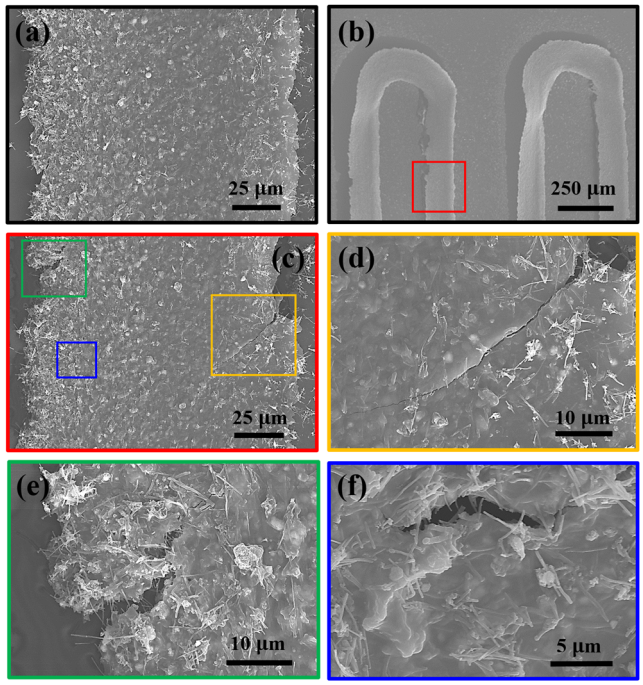

FIG. 4. SEM images of the printed nanocomposite (a) before and [(b) and (c)] after the fatigue test, where the enlarged images [(d)–(f)] show the microcracks formed within the nanocomposite after the prolonged fatigue test.

In summary, aerosol-jet printed, flexible, all-organic, and organic-inorganic hybrid composite thermoelectric devices were prepared incorporating materials such as conducting PEDOT:PSS polymers, high electrical conductivity MWCNTs, and high Seebeck coefficient Sb_2Te_3 nanoflakes. The introduction of MWCNTs and Sb_2Te_3 can also serve to lower the thermal conductivity by phonon scattering at the organic/inorganic interfaces for improved thermoelectric performance. To the best of our knowledge, these are some of the very first results where the aerosol-jet printing technique has been used to incorporate MWCNTs into flexible printed nanocomposite thermoelectric devices. A couple of important process modifications were implemented in these devices wherein *in situ* mixing of the component phases was used to form composite devices, the method potentially availing many advantages in printing advanced composite devices. The printed PEDOT:PSS-based nanocomposite devices were treated with different polar solvents to improve their σ by de-doping PSS. The results from the thermoelectric measurements across different compositions and surface treatments were compared, with the DMSO-treated Sb_2Te_3-MWCNTs-PVP-PEDOT:PSS nanocomposite showing the best PF of ~41 μW/mK^2 (S of ~29 μV/K and σ of ~496 S/cm). Furthermore, rigorous flexing and fatigue tests have proved the superior flexibility and robustness of these printed thermoelectric nanocomposites after 60 h continuous flexing cycles (36k cycles in total). Flexible thermoelectric nanocomposites with good durability as demonstrated in this work could find applications in thermal energy harvesters for wearable devices or in applications requiring ease of mounting and/or surface conformability of the energy harvester.

See supplementary material for details provided about (S1) description of the ink formulation for aerosol-jet printing; (S2) fabrication of aerosol-jet printed thermoelectric nanocomposites; (S3) the influence of surfactant addition on printed thermoelectric nanocomposites; (S4) thermoelectric measurement of printed thermoelectric nanocomposites; (S5) surface treatment on printed thermoelectric nanocomposites; and (S6) flexing test and fatigue test on printed thermoelectric nanocomposites.

This work was financially supported by a grant from the European Research Council through an ERC Starting Grant (Grant No. ERC–2014–STG–639526, NANOGEN). S.K.N. acknowledges support from the EPSRC grant "Centre for Advanced Materials for Integrated Energy Systems

(CAM-IES)" No. EP/P007767/1. A.S. is grateful for financial support from the Isaac Newton Trust. C.O. acknowledges studentship from the Cambridge Trust and China Scholarship Council. Q.J. is grateful for financial support through a Marie Sklodowska Curie Fellowship (No. H2020-MSCA-IF-2015-702868). Supporting data for this paper is available at the DSpace@Cambridge data repository (https://doi.org/10.17863/CAM.26050).

[1] M. Orrill and S. LeBlanc, J. Appl. Polym. Sci. **134**, 44256 (2017).
[2] C. B. Vining, Nat. Mater. **8**, 83 (2009).
[3] F. Suarez, A. Nozariasbmarz, D. Vashaee, and M. C. Öztürk, Energy Environ. Sci. **9**, 2099 (2016).
[4] A. J. Minnich, M. S. Dresselhaus, Z. F. Ren, and G. Chen, Energy Environ. Sci. **2**, 466 (2009).
[5] M. Zebarjadi, K. Esfarjani, M. S. Dresselhaus, Z. F. Ren, and G. Chen, Energy Environ. Sci. **5**, 5147 (2012).
[6] S. K. Yee, S. LeBlanc, K. E. Goodson, and C. Dames, Energy Environ. Sci. **6**, 2561 (2013).
[7] C. Ou, P. E. Sanchez-Jimenez, A. Datta, F. L. Boughey, R. A. Whiter, S.-L. Sahonta, and S. Kar-Narayan, ACS Appl. Mater. Interfaces **8**, 13678 (2016).
[8] A. Datta, A. Sangle, N. Hardingham, C. Cooper, M. Kraan, D. Ritchie, V. Narayan, and S. Kar-Narayan, Materials **10**, 553 (2017).
[9] C. Ou, A. L. Sangle, A. Datta, Q. Jing, T. Busolo, T. Chalklen, V. Narayan, and S. Kar-Narayan, ACS Appl. Mater. Interfaces **10**, 19580 (2018).
[10] B. Poudel, Q. Hao, Y. Ma, Y. Lan, A. Minnich, B. Yu, X. Yan, D. Wang, A. Muto, D. Vashaee, X. Chen, J. Liu, M. S. Dresselhaus, G. Chen, and Z. Ren, Science **320**, 634 (2008).
[11] M. S. Dresselhaus, G. Chen, M. Y. Tang, R. G. Yang, H. Lee, D. Z. Wang, Z. F. Ren, J.-P. Fleurial, and P. Gogna, Adv. Mater. **19**, 1043 (2007).
[12] L. D. Hicks and M. S. Dresselhaus, Phys. Rev. B **47**, 12727 (1993).
[13] D. Bhatia, S. Bairagi, S. Goel, and M. Jangra, J. Pharm. BioAllied Sci. **2**, 51 (2010).
[14] C. Yu, K. Choi, L. Yin, and J. C. Grunlan, ACS Nano **5**, 7885 (2011).
[15] O. Bubnova, Z. U. Khan, H. Wang, S. Braun, D. R. Evans, M. Fabretto, P. Hojati-Talemi, D. Dagnelund, J. Arlin, Y. H. Geerts, S. Desbief, D. W. Breiby, J. W. Andreasen, R. Lazzaroni, W. M. Chen, I. Zozoulenko, M. Fahlman, P. J. Murphy, M. Berggren, and X. Crispin, Nat. Mater. **13**, 190 (2014).
[16] Q. Wei, M. Mukaida, K. Kirihara, Y. Naitoh, and T. Ishida, Materials **8**, 732 (2015).
[17] B. Russ, A. Glaudell, J. J. Urban, M. L. Chabinyc, and R. A. Segalman, Nat. Rev. Mater. **1**, 16050 (2016).
[18] M. Culebras, C. Gómez, and A. Cantarero, Materials **7**, 6701 (2014).
[19] J. Yang, H.-L. Yip, and A. K.-Y. Jen, Adv. Energy Mater. **3**, 549 (2013).
[20] C. Bounioux, P. Díaz-Chao, M. Campoy-Quiles, M. S. Martín-González, A. R. Goñi, R. Yerushalmi-Rozen, and C. Müller, Energy Environ. Sci. **6**, 918 (2013).
[21] D. Kim, Y. Kim, K. Choi, J. C. Grunlan, and C. Yu, ACS Nano **4**, 513 (2010).
[22] W. Lee, Y. H. Kang, J. Y. Lee, K.-S. Jang, and S. Y. Cho, RSC Adv. **6**, 53339 (2016).
[23] G. P. Moriarty, J. N. Wheeler, C. Yu, and J. C. Grunlan, Carbon **50**, 885 (2012).
[24] J.-H. Bahk, H. Fang, K. Yazawa, and A. Shakouri, J. Mater. Chem. C **3**, 10362 (2015).
[25] D. Madan, Z. Wang, P. K. Wright, and J. W. Evans, Appl. Energy **156**, 587 (2015).
[26] Q. Wei, M. Mukaida, K. Kirihara, Y. Naitoh, and T. Ishida, RSC Adv. **4**, 28802 (2014).
[27] S. J. Kim, J. H. We, and B. J. Cho, Energy Environ. Sci. **7**, 1959 (2014).
[28] S. Shin, R. Kumar, J. W. Roh, D.-S. Ko, H.-S. Kim, S. Il Kim, L. Yin, S. M. Schlossberg, S. Cui, J.-M. You, S. Kwon, J. Zheng, J. Wang, and R. Chen, Sci. Rep. **7**, 7317 (2017).
[29] O. Bubnova, Z. U. Khan, A. Malti, S. Braun, M. Fahlman, M. Berggren, and X. Crispin, Nat. Mater. **10**, 429 (2011).
[30] Z. Lu, M. Layani, X. Zhao, L. P. Tan, T. Sun, S. Fan, Q. Yan, S. Magdassi, and H. H. Hng, Small **10**, 3551 (2014).
[31] G.-H. Kim, L. Shao, K. Zhang, and K. P. Pipe, Nat. Mater. **12**, 719 (2013).
[32] A. Chen, D. Madan, P. K. Wright, and J. W. Evans, J. Micromech. Microeng. **21**, 104006 (2011).
[33] M. Smith, Y. S. Choi, C. Boughey, and S. Kar-Narayan, Flexible Printed Electron. **2**, 015004 (2017).
[34] C. Biswas, K. K. Kim, H. Geng, H. K. Park, S. C. Lim, S. J. Chae, S. M. Kim, Y. H. Lee, M. Nayhouse, and M. Yun, J. Phys. Chem. C **113**, 10044 (2009).
[35] W. H. Duan, Q. Wang, and F. Collins, Chem. Sci. **2**, 1407 (2011).
[36] H. Menon, R. Aiswarya, and K. P. Surendran, RSC Adv. **7**, 44076 (2017).
[37] S. Liu, H. Deng, Y. Zhao, S. Ren, and Q. Fu, RSC Adv. **5**, 1910 (2015).
[38] J. Luo, D. Billep, T. Waechtler, T. Otto, M. Toader, O. Gordan, E. Sheremet, J. Martin, M. Hietschold, D. R. T. Zahn, and T. Gessner, J. Mater. Chem. A **1**, 7576 (2013).
[39] B. Fan, X. Mei, and J. Ouyang, Macromolecules **41**, 5971 (2008).
[40] A. M. Nardes, R. A. J. Janssen, and M. Kemerink, Adv. Funct. Mater. **18**, 865 (2008).
[41] S. Zhang, P. Kumar, A. S. Nouas, L. Fontaine, H. Tang, F. Cicoira, S. Zhang, P. Kumar, A. S. Nouas, and L. Fontaine, APL Mater. **3**, 014911 (2015).
[42] Z. Fan, D. Du, H. Yao, and J. Ouyang, ACS Appl. Mater. Interfaces **9**, 11732 (2017).
[43] S. Shin, J. W. Roh, H.-S. Kim, and R. Chen, J. Appl. Phys. **123**, 205106 (2018).
[44] E. E. Tkalya, M. Ghislandi, G. de With, and C. E. Koning, Curr. Opin. Colloid Interface Sci. **17**, 225 (2012).
[45] E. Jin Bae, Y. Hun Kang, K.-S. Jang, and S. Yun Cho, Sci. Rep. **6**, 18805 (2016).
[46] Y. Chen, M. He, B. Liu, G. C. Bazan, J. Zhou, and Z. Liang, Adv. Mater. **29**, 1604752 (2017).
[47] H. Song, C. Liu, J. Xu, Q. Jiang, and H. Shi, RSC Adv. **3**, 22065 (2013).
[48] C. Cho, K. L. Wallace, P. Tzeng, J.-H. Hsu, C. Yu, and J. C. Grunlan, Adv. Energy Mater. **6**, 1502168 (2016).